A PROTON THERAPY MODEL USING DISCRETE DIFFERENCE EQUATIONS WITH AN EXAMPLE OF TREATING HEPATOCELLULAR CARCINOMA

Erin N. Bodine* and K. Lars Monia†

Rhodes College
Department of Mathematics & Computer Science
2000 N. Parkway
Memphis, TN 38112, USA

(Communicated by Natalia Komarova)

Abstract. Proton therapy is a type of radiation therapy used to treat cancer. It provides more localized particle exposure than other types of radiotherapy (e.g., x-ray and electron) thus reducing damage to tissue surrounding a tumor and reducing unwanted side effects. We have developed a novel discrete difference equation model of the spatial and temporal dynamics of cancer and healthy cells before, during, and after the application of a proton therapy treatment course. Specifically, the model simulates the growth and diffusion of the cancer and healthy cells in and surrounding a tumor over one spatial dimension (tissue depth) and the treatment of the tumor with discrete bursts of proton radiation. We demonstrate how to use data from in vitro and clinical studies to parameterize the model. Specifically, we use data from studies of Hepatocellular carcinoma, a common form of liver cancer. Using the parameterized model we compare the ability of different clinically used treatment courses to control the tumor. Our results show that treatment courses which use conformal proton therapy (targeting the tumor from multiple angles) provides better control of the tumor while using lower treatment doses than a non-conformal treatment course, and thus should be recommend for use when feasible.

1. **Introduction.** Modern oncology provides a wide array of alternative cancer treatment options. With 1.6 million cases in the U.S. in 2014 and only 600,000 deaths, treatment capabilities are improving [29]. Treatment regimes are usually designed to balance the expedited removal/reduction of cancer cells with the quality of life and long term health of the patient.

One common form of cancer treatment is external beam radiotherapy, often referred to as just *radiation therapy*. In radiation therapy beams of x-rays (high energy photons), gamma rays, or other charged particles are fired into the body of a patient at a specifically targeted point. As the beam passes through tissue the DNA of cells are damaged, typically resulting in cell death. Note that the cell death does not occur instantaneously as the radiation is applied. Depending on the type of cell, it may take several hours or even days before the damaged cells begin to die.

By firing the beam multiple times from different angles, referred to as *conformal radiation therapy*, radiation oncologists can cause significant damage to cancer cells [27]. Though damage is done to both cancer cells and surrounding healthy cells, the aim of radiation therapy is to kill cancer cells while minimizing damage to healthy cells [27, 22, 20].

Proton therapy is a form of radiation that uses a particle accelerator to form a beam of high energy protons that are fired into the patient to irradiate cancer cells. The advantage of proton therapy is that it provides more localized treatment and allows for higher dose treatments for patients than radiation therapy using photons. As shown in Figure 1 and first observed by Bragg and Kleenman [10], charged particle beams of proton mass deliver the majority of their dose (energy per unit mass) at a depth near the end of their range and over a narrow depth range (about 0.5-1.0 cm) known as the *Bragg peak region* [20, 35, 22, 2]. For a single Bragg peak curve, the depth at which the maximum dosage is received, called the *target depth*, can be controlled by altering the initial energy generated by the particle accelerator forming the proton beam. Note that the amount of dosage received at tissue depths greater than the target depth quickly fall off to zero.
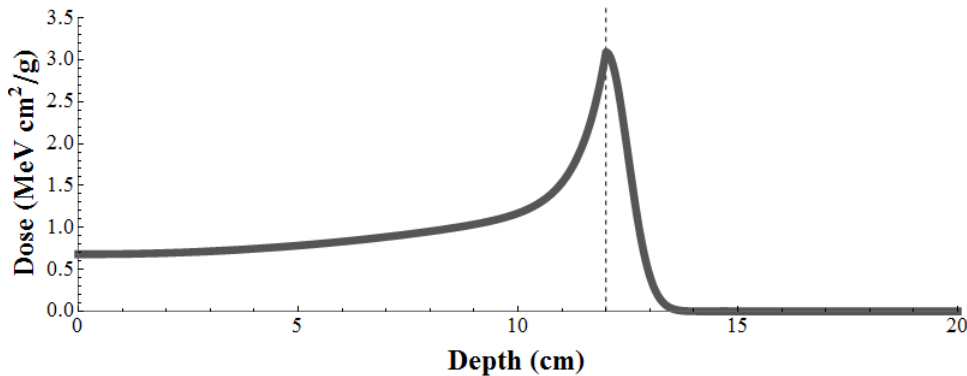

FIGURE 1. Dose delivered by a single proton beam targeted at a depth of 12 cm (shown by the dashed line).

The narrowness of the Bragg peak, and the relatively low dose outside the Bragg peak region prompted Wilson in 1946 [37] to suggest the use of protons for radiation therapy as a means of minimizing damage to tissue surrounding a tumor site, and the first patient treated with proton therapy was in 1954 at the Lawrence Berkeley Laboratory [27, 2]. Since then it has been observed that proton therapy results in a higher probability of tumor control and patient tolerance (i.e., less negative side-effects) than treatment with photon therapy [27]. Due to the ability of proton therapy to target a narrow region, the use of proton therapy has been of particular interest in treating tumors growing in close proximity to what are called *serially organized tissues* in which damage to a small portion of this type of tissue will have secondary effects on adjacent tissue such that normal function may cease [21, 27], for example the spinal chord. Proton therapy has been used to treat tumors located in a variety of locations, including the paranasal sinus [31], the prostate [16, 30], the brain [18], the base of the skull [34], and the liver [11].

Since the mass of a typical tumor targeted with proton therapy is wider than the Bragg peak region of a single proton beam, to treat the entire tumor a proton beam

is modulated to create a *spread out Bragg peak* (SOBP) [22]. Modulation is achieved through a sequence of absorbers, each creating a single Bragg peak curve with the sequential set of Bragg peaks occurring at decreasing depths and with decreasing relative dosage [27]. Figure 2 shows a SOBP which is the sum of the sequence of Bragg peak curves shown. A typical treatment session involves the firing of one or more modulated proton beams [27]. If multiple modulated beams are fired, each beam targets the tumor from a different angle in a treatment method known as *conformal proton therapy*.
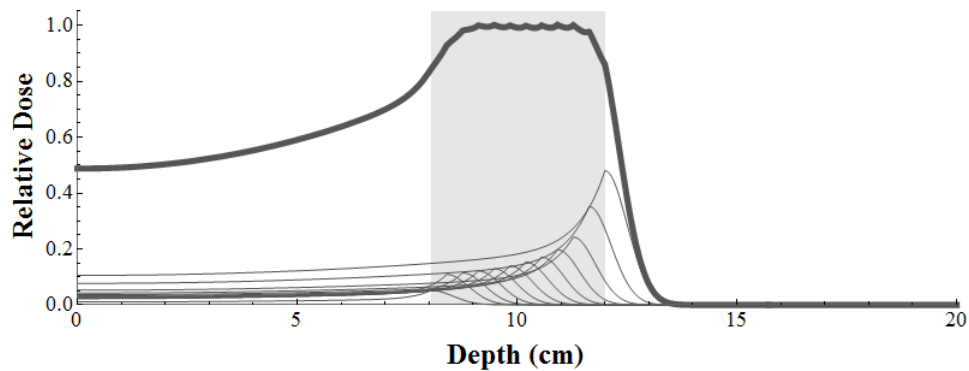

FIGURE 2. The relative dose of a SOBP curve (thick curve) comprised of 12 Bragg peaks (thin curves). The shaded region shows the range of targeted depths.

Due to the fact that the relative dose of a proton therapy treatment is heterogeneously delivered over a range of depths, we have developed a spatially explicit model to examine the effects of proton therapy upon a tumor mass and surrounding tissue. Specifically, we have formulated a discrete difference equation patch model with discrete diffusion to simulate tumor growth over one-dimensional space and with discrete bursts of applied proton therapy. Using this model we examine the effects of applying proton therapy multiple times over a period of several weeks (a single *treatment course*). The development of our model builds off of existing models of linear cancer networks [36, 23] which are briefly described in Section 2. A detailed description of our proposed model and assumptions are given in Section 3. In Section 4 we describe how the model is parameterized using data from in vitro and clinical studies. As an example, we parameterize the model for the treatment of Hepatocellular carcinoma, a common form of liver cancer. In Section 5 we describe and compare the results of simulations. We examine one treatment course of non-conformal proton therapy and two different conformal proton therapy treatment courses. Finally, in Section 6 we consider the implication and impact of our results, discuss the potential drawbacks of our proposed model, and consider some future extensions to the proposed model.

2. **Linear cancer networks.** In 2011, Werner proposed a general theoretical framework describing all possible cancer networks [36]. Werner's new paradigm presents many open research problems, and much work remains to be done in translating these abstract networks into descriptive implementations such as differential equation or discrete difference equation models in order to simulate and

quantify the impact of radiation and other therapies. Linear cancer networks, one of the conceptual frameworks of tumor growth developed by Werner [36], allows for a simplified approach to modeling tumor development. A tumor is assumed to begin with cancer stem cells (denoted as A cells) which differentiate to produce non-proliferating cancer cells (denoted as B cells). It is assumed the B cells amass to form the bulk of the tumor. A single A cell, however, will continue differentiating, producing more and more B cells.

Let $A(t)$ be the number of A cells at time t, and $B(t)$ be the number of B cells at time t. The initial model of a linear cancer network proposed by Werner [36] assumed the number of A cells remained constant, while the growth rate of B cells increased linearly with respect to the number of A cells (hence the name *linear cancer networks*). This simple model is described by $dA/dt = 0$ and $dB/dt = k_A A$, where k_A is the differentiation rate for the B cells. Manley [23] expanded on the model proposed by Werner by adding the cells of healthy tissue, $H(t)$, to the model, and allowing logistic growth of the cancer cells which is justified by previous research on tumor growth rates (see [32] for details). This expanded model is described by

$$\frac{dA}{dt} = k_A A \left(1 - \frac{A}{M_A}\right) - r_A \tag{1a}$$

$$\frac{dB}{dt} = k_A A \left(\frac{A}{M_A}\right)\left(1 - \frac{B}{M_B}\right) - \delta B - r_B \tag{1b}$$

$$\frac{dH}{dt} = k_H H \left(1 - \frac{H}{M_H}\right) - r_H, \tag{1c}$$

where M_A, M_B, and M_H represent the carrying capacities of the A, B, and H cells in a given tissue volume, respectively; k_A and k_H are the intrinsic growth rates of the cancer and healthy cells, respectively; δ is the natural death rate of tumor cells; and r_A, r_B, and r_H are constant death rates due to radiation therapy. Manley uses the model to explore the effects of both photon and proton radiation therapy, but the assumption of a continuous application of the therapy and a spatially homogeneous dosage is unrealistic. Thus, we propose a spatial explicit model where the application of proton therapy is applied in discrete bursts.

3. **Model description & assumptions.** The model we propose builds on the Werner-Manley model given in System (1). However, our model is discrete in time and space (using discrete difference equations), uses diffusion to simulate tumor growth, and allows for the repeated application of proton radiation in discrete bursts. Our model uses a depth-range targeted SOBP to simulate the application of proton radiation and assumes cell death over time due to a single application of proton radiation is modeled by a Gaussian distribution function.

Let A_t^i, B_t^i, and H_t^i be the densities of A, B, and H cells respectively at time t and depth i, where $t, i \in \mathbb{N}$. Each time step t represents 1 hour, and each depth i represents a layer of tissue 1 mm thick. Let P_t^i be the relative dose of proton therapy at time t and depth i. We assume that cancer stem cells and healthy cells will diffuse from tissue depths of high concentration to tissue depths of low concentration, and use the formulation for discrete diffusion described in [15]. Since the Werner-Manley model of the linear cancer networks assumes the amassing of B cells, we consider the diffusion of B cells to be negligible. Our model is given by

$$A_{t+1}^i = A_t^i + k_A A_t^i \left(1 - \frac{A_t^i}{M_A}\right) - A_t^i P_t^i + d_A \sum_{j=0}^{n} (A_t^j - A_t^i) e^{-(j-i)^2/\mu_A} \tag{2a}$$

$$B_{t+1}^i = B_t^i + k_A A_t^i \left(\frac{A_t^i}{M_A}\right) \left(1 - \frac{B_t^i}{M_B}\right) - B_t^i P_t^i \tag{2b}$$

$$H_{t+1}^i = H_t^i + k_H H_t^i \left(1 - \frac{H_t^i}{1 - A_t^i - B_t^i}\right) - H_t^i P_t^i + d_H \sum_{j=0}^{n} (H_t^j - H_t^i) e^{-(j-i)^2/\mu_H}, \tag{2c}$$

where M_A, M_B represent the relative carrying capacities of the A and B cells respectively, and k_A and k_H are the intrinsic growth rates of the cancer and healthy cells, respectively. Note that for any given tissue depth i, $A_t^i + B_i^t + H_t^i \leq 1$, and thus the maximum density at tissue depth i is 1 cell per unit area. The effective rates of diffusion for A and H cells are given by parameters μ_A and μ_H, respectively, and the diffusion coefficients d_A and d_H are defined as

$$d_A = \left(\sum_{i=0}^{n}\sum_{j=0}^{n} \left(e^{-(j-i)^2/\mu_A}\right)\right)^{-1} \text{ and } d_H = \left(\sum_{i=0}^{n}\sum_{j=0}^{n} \left(e^{-(j-i)^2/\mu_H}\right)\right)^{-1}.$$

For a given time t, let τ be the set of previous times at which proton therapy has been applied. Then

$$P_t^i = \alpha \sum_{t^* \in \tau} \left[\mathcal{D}_{t^*}^i e^{-\beta(t-t^*-\delta)^2}\right], \tag{2d}$$

where α is the maximum cell death rate at tissue depth i due to a single proton treatment, $\mathcal{D}_{t^*}^i$ is the relative dose at depth i and time t^* due to the treatment applied at time t^*, δ is the number of hours after t^* at which the cell death rate is maximized due to treatment applied at t^*, and β determines the time range over which the majority of cell death occurs. The relative dose $\mathcal{D}$ over all tissue depths is defined by a clinical approximation of the solution to the Bethe-Block Equation which simulates a Bragg-Peak curve (see Section 3.1). Note that the formulation of P_i^t allows for the delayed effect of proton therapy treatment applied at a previous time step to combine with the effect of treatment applied at a later time step thus accounting for the delayed effect of a proton therapy treatment on cell death.

3.1. Bethe-Bloch equation.

High energy particles such as protons and photons damage tissue through which they travel in distinct patterns defined by their stopping power. As a particle travels through a given material, it may collide with the molecules or cells of that material, releasing a portion of its energy. The stopping power of a charged particle, $S(z)$, is defined to be the amount of energy at depth z a given material will receive when high energy particles pass through it [10, 33]. The Bethe-Bloch formula, explained in detail in [38], gives the stopping power of a given system of excited particles through a given material. However, in a clinical setting, the stopping power, and the dose at each depth, is determined from an approximate solution to the Bethe-Bloch equation, which we will refer to as a *clinical solution*.

3.1.1. *A clinical solution for the Bethe-Bloch equation.*

We use the clinical solution of the Bethe-Bloch equation developed by Ulmer and Schaffner [33] to represent the stoppage power (and thus the dose) of the protons at various tissue depths. Let R

be the target depth. The initial energy generated by the particle accelerator, E_0, is defined as a function of R [7],

$$E_0 = \left(\frac{R}{0.0022}\right)^{1/1.77}. \tag{3}$$

The dosage at depth z given target depth R, $S(z, R)$, is approximated by

$$S(z, R) \approx \sum_{n=1}^{6} \phi_n(z, R), \tag{4}$$

where the functions $\phi_i(z, R)$ are defined as

$$\phi_1(z, R) = C_1 \exp\left(-\left(\frac{R-z}{\tau_0}\right)^2\right)\theta(z) \tag{5a}$$

$$\phi_2(z, R) = 2C_2\,\theta(z) \tag{5b}$$

$$\phi_3(z, R) = 2C_3 \exp\left(-Q_p\left(R-z\right)\right)\theta(z) \tag{5c}$$

$$\phi_4(z, R) = 2C_4\left(\frac{z}{R}\right)^2\theta(z) \tag{5d}$$

$$\phi_5(z, R) = 2C_5\left(1-\frac{z}{R}\right)\theta(z) \tag{5e}$$

$$\phi_6(z, R) = \left(\sum_{i=2}^{5}\phi_n(R, R)\right)\exp\left(-2(z-R)^2\right)\psi(z). \tag{5f}$$

The coefficients C_i for $i = 1, \ldots, 6$, and Q_p are functions of E_0 (and thus functions of the target depth R) and are given in Table 1. The functions $\theta(z)$ and $\psi(z)$ are step functions defined by

$$\theta(z) = \begin{cases} 1, & z \leq R \\ 0 & z > R \end{cases} \text{ and } \psi(z) = \begin{cases} 0, & z \leq R \\ 1 & z > R \end{cases}. \tag{6}$$

Note that $z = R$ is the depth at which maximum dosage is received, and that the functions $\phi_1(z), \ldots, \phi_5(z)$ provide the approximation of $S(z, R)$ for $0 \leq z \leq R$, while the function $\phi_6(z)$ provides the approximation of $S(z, R)$ for $z \geq R$. The Bragg peak curves in Figures 1 and 2 are generated using this approximation.

TABLE 1. Coefficients and parameters for clinical approximation of the Bethe-Bloch formula (Equations (4)-(6)) as given in [33].

Parameter	Value	Parameter	Value
C_1	$2.277463 - 0.0018473E_0$	C_2	$0.243100 - 0.0007000E_0$
C_3	$1.029500 - 0.0010300E_0$	C_4	$0.405300 - 0.0007000E_0$
C_5	0.007000	τ_0	10^{-5}
Q_p	$\dfrac{\pi(6.267510 + 0.0010300E_0)}{R\left(1 + (2.11791 \times 10^{-5})\,E_0 + (0.9192399 \times 10^{-7})\,E_0^2\right)}$		

3.1.2. *Formulating a spread Out Bragg peak (SOBP).* A SOBP curve is formed as a weighted sum of multiple Bragg peak curves. A method for determining the weights of each single Bragg peak curve was developed by Bortfeld [8], and refined by Jette and Chen [17]. For a SOBP created using $n + 1$ Bragg peak curves distributed over a target region $[(1 - \chi)R_{\max}, R_{\max}]$, the target depth of the kth curve is given by

$$R_k = \left[1 - \left(1 - \frac{k}{n}\right)\chi\right] R_{\max}, \text{ for } k = 0, 1, \ldots, n, \tag{7}$$

and thus the kth Bragg peak curve is given by $S(z, R_k)$. Note that $R_0 = R_{\max}$, $R_n = (1 - \chi)R_{\max}$, and χ represents the proportion of the region $[0, R_0]$ which is targeted. The SOBP curve represents the dose at tissue depth z (in MeV cm^2/g) and is defined as

$$D(z, R_{\max}, \chi) = \sum_{k=0}^{n} w_k S(z, R_k), \tag{8}$$

with each weight w_k defined by

$$w_k = \begin{cases} 1 - \left(1 - \frac{1}{2n}\right)^{1-1/p} & k = 0 \\ \left[1 - \frac{1}{n}\left(k - \frac{1}{2}\right)\right]^{1-1/p} - \left[1 - \frac{1}{n}\left(k + \frac{1}{2}\right)\right]^{1-1/p} & 1 \le k \le n - 1 \\ \left(\frac{1}{2n}\right)^{1-1/p} & k = n, \end{cases} \tag{9}$$

where the parameter p is adjusted to keep the dose over target region relatively constant. Note that Figure 2 shows a SOBP composed of 12 Bragg peak curves ($n = 11$) with $R_{\max} = 12$ cm, $\chi = 0.3$, and $p = 2$.

For our model (System (2)), the relative dose at depth i due to treatment applied at time step t^* is approximated by

$$\mathcal{D}_{t^*}^i = \frac{D\left(\frac{z(i) + z(i+1)}{2}, R_{\max}, \chi\right)}{D_{\max}} \tag{10}$$

where $z(i)$ is the tissue depth (in cm), and $D_{\max} = \max_{z}[D(z, R_{\max}, \chi)]$. Note that the relative dose for tissue depth i is calculated at the midpoint of the ith subinterval $[i, i + 1]$.

4. **Model parameters for a case of hepatocellular carcinoma.** As a sample case, we have used parameters which describe the growth and treatment of *Hepatocellular carcinoma (HCC)*, a common form of liver cancer. Proton therapy has been used to treat HCC, but there remains a need for research and clinical trials to determine the effects of proton therapy used alone and with other treatment options [13]. Using the model proposed in Section 3 with parameters which describe the growth of liver cells (hepatocytes) and the impact of proton therapy on HCC we are able to examine the temporal and spatial effects of treating HCC with proton therapy alone.

All parameters used for the numerical simulation of the growth and treatment of HCC tumors are given in Table 2, with their derivation and/or biological motivation described in detail through the remainder of this section.

4.1. **Parameters defining spatial & temporal scales.** We assume that each depth i represents a layer of tissue 1 mm thick. For the simulations shown in Section 5, we use a spatial domain of 20.1 cm, i.e. $i \in 0, 1, \ldots, 200$. Additionally, each time step t represents the passing of 1 hour.

TABLE 2. Values of parameters used in simulations of the model described in Section 3.

Parameter		Value
k_A	Cancer cell growth rate (hours^{-1})	0.008 165
k_H	Healthy cell growth rate (hours^{-1})	2.108 703
M_A	Relative carrying capacity of A cells in 1 mm layer of tissue	0.225
M_B	Relative carrying capacity of B cells in 1 mm layer of tissue	0.675
μ_A	Effective diffusion rate for A cells	0.133 642
μ_H	Effective diffusion rate for H cells	0.131 166
α	Maximum cell death rate at depth i from a single treatment	0.02
β	Determines range over which the majority of cell death occurs	0.0075
δ	Hours after treatment at which cell death rate is maximized	47

4.2. **Instrinic growth & effective diffusion rates of H cells.** In the absence of cancer cells, when a portion of the liver is surgically removed, the liver cells will regenerate quickly (see liver regeneration studies [25, 24, 14] for details). Together, the parameters k_H (the intrinsic growth rate of H cells) and μ_H (the effective diffusion rate of H cells) determine how quickly healthy tissue is able to regenerate across the spatial domain. To determine appropriate values of k_H and μ_H we used data for liver cell regeneration provided by Nagasue, et al. [25]. In this study, five patients with normal livers (no chirrosis or chronic hepatitis) had right lobectomies where 60% of the volume of their liver was removed leaving 40% of each patient's original liver volume directly after surgery. Averaging across the five patients, after 8 days liver volumes had recovered to 49% of the original liver volumes, and after 100 days liver volumes had recovered to 98% of the original liver volumes.

To determine the values of k_H and μ_H which would best approximate the averaged patient data presented by Nagasue, et al. [25] we use Latin Hypercube sampling to generate 2000 pairs of (k_H, μ_H) assuming possible values of k_H and μ_H to be uniformly distributed over $[0.0005, 3]$ and $[0.05, 3]$, respectively (see [5, 4, 6] for details and examples of Latin Hypercube sampling). Next, we simulate System (2) with no cancer cells (i.e., $A_t^i = B_t^i = 0$ for all i and t) and no proton therapy treatment over 100 days (2400 times steps) for each of the (k_H, μ_H) parameter pairs. Each simulation uses a healthy cell initial condition of

$$H_0^i = \begin{cases} 1 & i = 0, \dots, 80 \\ 0 & i = 81, \dots, 200 \end{cases},$$

i.e., we start with 40% of the total possible volume of healthy cells. Lastly, we select k_H and μ_H such that

$$\min_{k_H, \, \mu_H} \sqrt{(\boldsymbol{H_{192}} - 0.49)^2 + (\boldsymbol{H_{2400}} - 0.98)^2} \text{ where } \boldsymbol{H_t} = \frac{1}{201} \sum_i H_t^i.$$

This process yields the parameter values $k_H = 2.108703$ and $\mu_H = 0.131166$. Note that 8 days is 192 time steps and 100 days is 2400 times steps.

4.3. **Relative carrying capacities.** Recall that System (2) is constructed such that $A_t^i + B_t^i + H_t^i \leq 1$. We further assume that the relative carrying capacities of A and B cells at tissue depth i is $M_A + M_B < 1$, thus a particular layer can become mostly cancer cells, but cannot be composed entirely of cancer cells. Next, an underlying assumption of linear cancer networks is that A cells proliferate, while B cells accumulate. Thus, we assume that $M_B > M_A$. Specifically for the results shown in Section 5 we assume $M_A + M_B = 0.9$ and $M_B = 3M_A$, which together yield $M_A = 0.225$ and $M_B = 0.675$.

4.4. **Instrinic growth & diffusion rates of A cells.** The tumor volume doubling time (TVDT) of HCCs varies greatly. In a study of 15 patients with small (< 5 cm in diameter) HCC tumors by Okazaki, et al. [26] the range in TVDTs was 39–305 days with mean 102 ± 77 days. In study of 39 patients with small (< 5 cm in diameter) HCC tumors by Barbara, et al. [3] the range in TVDTs was 27–605 days with mean of 204 ± 135 days. For parameterization of System (2) we assumed a TVDT of 150 days. A doubling in tumor volume is assumed to be equivalent to a doubling in cancer cell density. Thus, if we let

$$C_t = \frac{1}{201} \sum_i \left(A_t^i + B_t^i \right)$$

be the average cancer density across all tissue depths at time t, then after 150 days ($t = 3600$) we expect

$$C_{3600} = 2C_0. \tag{11}$$

However, since Model 2 accounts for only one spatial dimension, if we assume the HCCs develop in a volume that can be approximated by sphere, then for a tumor with diameter d_0 at time $t = 0$, the diameter t days later will be

$$d_t \approx d_0 \times 10^{t/(10\ T_D)}, \tag{12}$$

where T_D is the tumor volume doubling time. For example, if $T_D = 150$ and the tumor is 30 mm in diameter at $t = 0$ (i.e., $d_0 = 30$), then after 150 days ($t = 3600$) the tumor will have a diameter of 38 mm (i.e., $d_{3600} = 38$).

For the purpose of measurement, we assume that tissue depths with $A_t^i + B_t^i \geq 0.55$ are "visible" as part of the tumor, and thus contribute to the diameter of the tumor. To determine parameter combinations that would result in a tumor volume doubling time of 150 days, we start with a visible 30 mm tumor located in the center of the spatial domain. Specifically, we use initial conditions

$$A_0^i = \begin{cases} 0.1375 & i = 85, \ldots, 114 \\ 0 & \text{otherwise} \end{cases}, \quad B_0^i = \begin{cases} 0.4125 & i = 85, \ldots, 114 \\ 0 & \text{otherwise} \end{cases}, \text{ and}$$

$$H_0^i = 1 - A_0^i - B_0^i.$$

Notice, for $i = 85, \ldots, 114$, $A_0^i + B_0^i = 0.55$ and $B_0^i = 3A_0^i$.

To determine values of k_A and μ_A for which $C_{3600} \approx 2C_0$ and $d_{3600} = 38$, we again use Latin Hypercube sampling to generate 1000 pairs of (k_A, μ_A) assuming possible values of k_A and μ_A to be uniformly distributed over $[0.0005, 0.1]$ and $[0.05, 1.0]$, respectively. Next, we simulate System (2) with no proton therapy treatment over 150 days (3600 times steps) for each of the 1000 (k_A, μ_A) parameter pairs. Lastly, we select the (k_A, μ_A) parameter pair such that $d_{3600} = 38$ and

$$\min_{k_A,\ \mu_A} \left| \frac{C_{3600}}{C_0} - 2 \right|.$$

This process yields the parameter values $k_A = 0.008165$ and $\mu_A = 0.133642$ and result in $\mathbf{C_{3600}} = 2.037\mathbf{C_0}$ and $d_{3600} = 38$.

4.5. **Parameters for application of proton therapy.** Proton radiation damages the DNA of cells, but does not cause the immediate cell death. An experiment by Lee, et al. [19] on the effects of proton therapy on HCC cell death found that in a culture of HCC cells exposed to a 5 Gy dose proton beam (a typical patient dose) there was virtually no effect on cell death during the first 24 hours, but only about 66.5% of the cells were alive after 72 hours. If the dose was lowered to 2 Gy, there was still virtually not effect on cell death during the first 24 hours, and 74.7% of the cells were alive after 72 hours. Since Lee, et al. [19] do not provide data on cell death after 72 hours, for both doses we have assumed the increase in cell death after 72 hours is minimal.

We approximate the HCC cell death rate at time t and tissue depth i from a single proton therapy treatment applied at time $t = 0$ by the function

$$f(t) = \alpha e^{-\beta(t-\delta)^2}, \tag{13}$$

where α is the maximum cell death rate at depth i from a single treatment, δ is the hours after a single treatment at which the cell death rate is maximized, and β defines the range over which the majority of the cell death occurs. Let x_t be the proportion of the initial HCC cell culture left after time t. If a single treatment of proton therapy is applied at $t = 0$, then

$$x_{t+1} = x_t(1 - f(t)). \tag{14}$$

Using Equation (14), we determined estimates for α, β, and γ that fit the data for both the 5 Gy and 2 Gy dose experiments performed by Lee, et al [19].

5 Gy Dose: Parameter values $\alpha = 0.020$, $\beta = 0.00750$, and $\delta = 47$ yield $x_{24} = 0.999$, $x_{72} = 0.663$, and $x_{100} = 0.662$ which approximates the data from Lee, et al. [19] for a 5 Gy dose.

2 Gy Dose: Parameter values $\alpha = 0.015$, $\beta = 0.00845$, and $\delta = 50$ yield $x_{24} = 1.000$, $x_{72} = 0.748$, and $x_{100} = 0.748$ which approximates the data from Lee, et al. [19] for a 2 Gy dose.

Figure 3 shows the time dependent cell death rate at a particular tissue depth due to a single applications of proton therapy treatment using a 5 Gy dose (solid cure) and a 2 Gy dose (dashed curve).

5. **Numerical simulations of growth & treatment of an HCC tumor.** The parameter values used for each of the simulations discussed here are given in Table 2. Note a single treatment course refers to a set of proton therapy treamtents given to a patient over a 1–2 month period after which there is a period of no treatment so that the patient can recover from any adverse side effects of the treatment. After the period of no treatment the patient is usually re-evaluated to determine how much of the cancer remains.

5.1. **Non-conformal treatment course.** To simulate the effects of a typical (non-conformal) proton therapy treatment course given to a HCC patient we used a treatment course (multiple doses of proton therapy administered over several weeks) similar to those reported by a retrospective review of proton therapy treatment in 162 HCC patients [11]. Of the 162 patients, the median dose given to a patient was 4.5 Gy, however dose size ranged from 2.9–6.0 Gy. Patients received 10–24 doses over 13–50 days. Typically, the larger the dose size, the fewer doses given.
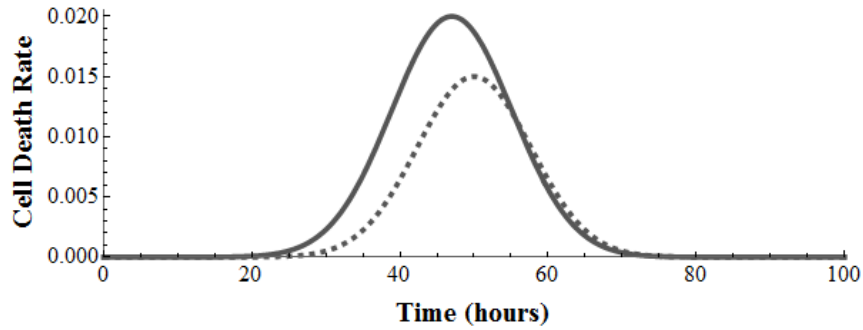
FIGURE 3. Time dependent cell death rate at tissue depth i due to a single proton therapy treatment as described by Equation (13) with $\alpha = 0.020$, $\beta = 0.00750$, and $\delta = 47$ for 5 Gy dose (solid curve) and $\alpha = 0.015$, $\beta = 0.00845$, and $\delta = 50$ for 2 Gy dose (dashed curve).

Of the 162 patients, the treatment course given most often was a dose of 4.5 Gy given 16 times over the course of 24 to 43 days. Since the data we used for time dependent cell death rate used a 2.0 Gy dose and a 5.0 Gy dose, we approximated this treatment course with a dose schedule of 5.0 Gy given 16 times over 35 days (5 weeks) with the dosing schedule as shown in Table 3(a). Note a total of 80 Gy of proton radiation are administered over the 5 weeks.

TABLE 3. Proton therapy treatment course of (a) 16 doses over 35 days (5 weeks), and (b) 20 doses over 49 days (7 weeks). The number in each box indicates the day of the treatment course and shaded boxes indicate the days on which treatment is administered.

(A) 5 week treatment course

Week	S	M	T	W	T	F	S
1	1	2	3	4	5	6	7
2	8	9	10	11	12	13	14
3	15	16	17	18	19	20	21
4	22	23	24	25	26	27	28
5	29	30	31	32	33	34	35

(B) 7 week treatment course

Week	S	M	T	W	T	F	S
1	1	2	3	4	5	6	7
2	8	9	10	11	12	13	14
3	15	16	17	18	19	20	21
4	22	23	24	25	26	27	28
5	29	30	31	32	33	34	35
6	36	37	38	39	40	41	42
7	43	44	45	46	47	48	49

The simulation uses initial conditions

$$A_0^i = \begin{cases} 0.1375 & i = 85, \ldots, 114 \\ 0 & \text{otherwise} \end{cases}, \quad B_0^i = \begin{cases} 0.4125 & i = 85, \ldots, 114 \\ 0 & \text{otherwise} \end{cases}, \quad \text{and}$$

$$H_0^i = 1 - A_0^i - B_0^i.$$

Notice, for $i = 85, \ldots, 114$, $A_0^i + B_0^i = 0.55$ and $B_0^i = 3A_0^i$. The simulation allows the tumor to grow for 150 days (3600 times steps), and Day 1 of the treatment schedule begins on Day 151 of the simulation. We assume that treatment is given at noon each day it is scheduled, thus the first dose is administered at noon on Day 152 of the simulation (time step $t = 152 \times 24 + 12 = 3660$). After the 35 day treatment period, the simulation continues another 90 days (without treatment) to allow for observation of tumor growth after treatment. Thus, the entire simulation is 275 days (6600 time steps).

The results of the simulation are shown in Figures 4(a) and 4(b). Again, for the purposes of measurement, we assume that tissue depths with $A_t^i + B_t^i \geq 0.55$ are "visible" as a part of the tumor, and thus contribute to the diameter of the tumor, d_t. At the beginning of the simulation the cancer cells (A and B cells) only exist at tissue depths $i = 85, \ldots, 114$ making the diameter of the tumor 30 mm ($d_0 = 30$). After 150 days of no treatment, there are 2.037 times as many cancer cells present as at the start of the simulation ($\boldsymbol{C_{3600}} = 2.037\ \boldsymbol{C_0}$, using the notation of Section 4), and the diameter of the visible tumor has grown to 38 mm ($d_{3600} = 38$). After the 35 day treatment period, there are 0.062 times as many cancer cells present as at Day 150 ($\boldsymbol{C_{4440}} = 0.062\ \boldsymbol{C_{3600}}$, nearly a 94% reduction in cancer cell density), and the diameter of the visible tumor has shrunk to 0 mm ($d_{4440} = 0$). Though this result seems promising, after the additional 90 day observation period, there are 1.188 times as many cancer cells present as at Day 150 ($\boldsymbol{C_{6600}} = 1.188\ \boldsymbol{C_{3600}}$, almost a 19% increase in cancer cell density when compared to right before treatment), and the diameter of visible tumor has increased to 44 mm ($d_{6600} = 44$). These results are summarized in Table 4. Note, if no proton therapy treatment had been given over the 35 day treatment period, then by Day 275 there would be 1.236 times as many cancer cells present as at Day 150 ($\boldsymbol{C_{6600}} = 1.236\ \boldsymbol{C_{3600}}$) and the diameter of visible tumor would have increased to 46 mm ($d_{6600} = 46$). This means, the patient is only slightly better off for having undergone the treatment.

In Figure 4(b) we see the healthy cells quickly rebound into the tumor region during and shortly after treatment, but as the observation period progresses the healthy cells are removed from the tumor region as the tumor re-establishes itself. Upon close inspection of Figure 4(b), a shaded triangle centered around the tumor can be seen. Figure 5 shows a close up of a portion of this region from Figure 4(b). Specifically, it shows tissue depths $i = 75, \ldots, 90$ for the first 6 hours of Day 30 of the simulation, that is $t = 721, \ldots, 726$. The checkerboard pattern that forms is a result of the combination of the diffusion of healthy cells and the overcrowding effects of logistic growth. For clarity, in hours 1 and 2 of Day 30 ($t = 721$ and $t = 722$) boxes are formed around three tissue depths: 75 mm, 79 mm, and 82 mm. The values shown in each box indicate the value of H_t^i at that time and tissue depth. Notice, within the checkerboard patterned region the density of healthy cells are switching to values above 1 (the carrying capacity of any single tissue depth) and below 1. When a particular tissue depth gains a healthy cell density greater than 1, diffusion will move healthy cells out of that depth to lower density depths (darker shaded cells) and the overcrowding effects of logistic growth with eliminate cells from that tissue depth causing a lower cell density at that tissue depth in the next time step. Conversely, when the healthy cell density at a particular tissue depth is below 1, diffusion will move healthy cells from higher density depths (lighter shaded cells) into that tissue depth, and the logistic growth will additionally cause the production of some new healthy cells. Together, the effects of diffusion and

(A) Cancer cells $(A + B)$; Non-conformal treatment

(B) Cancer cells (H); Non-conformal treatment

(C) Cancer cells $(A+B)$; Conformal treatment A

(D) Cancer cells (H); Conformal treatment A

(E) Cancer cells $(A+B)$; Conformal treatment B
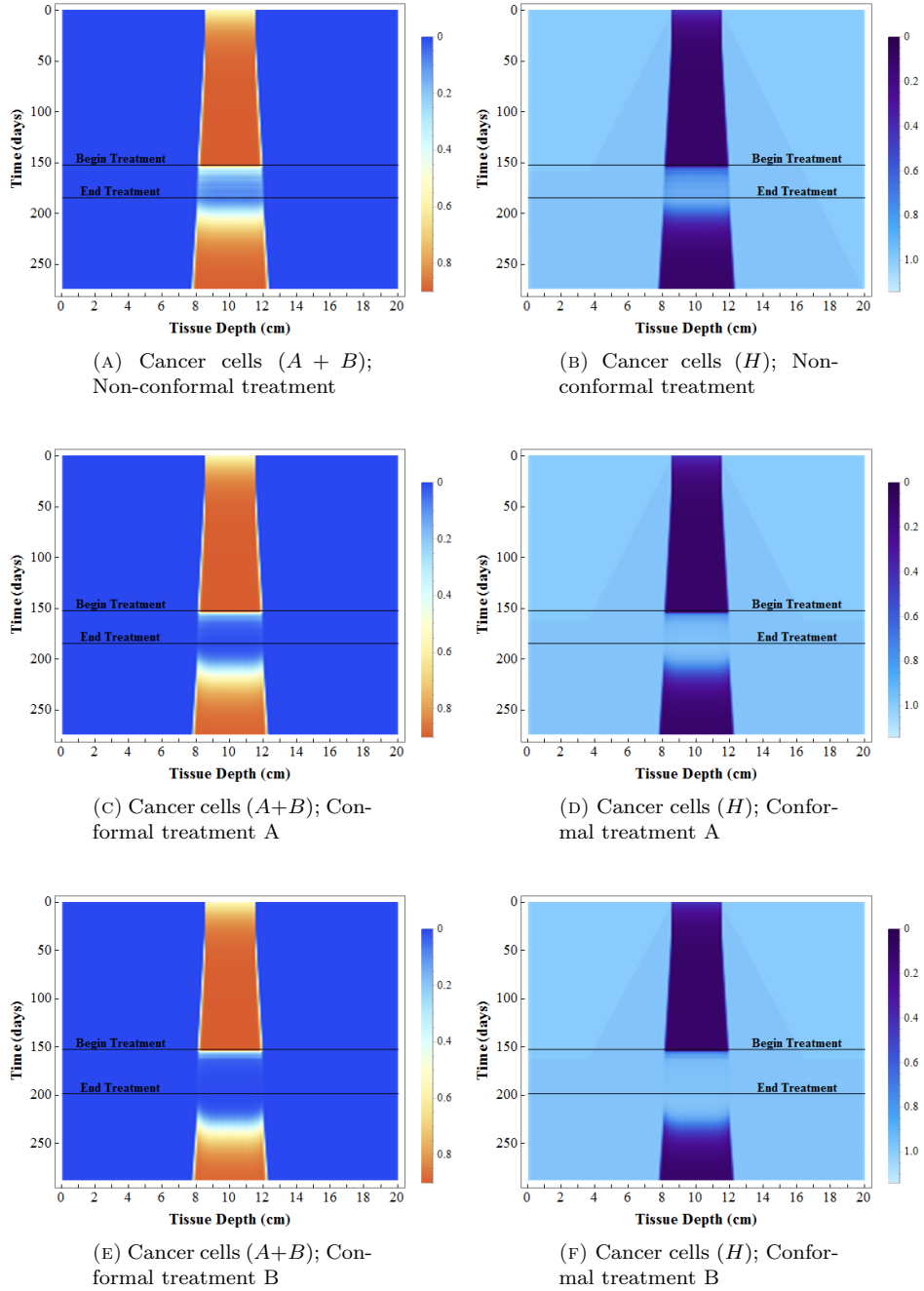
(F) Cancer cells (H); Conformal treatment B

FIGURE 4. Simulation of the growth and treatment of a hepatocellular carcinoma for each of the treatment courses: non-conformal (top row), conformal A (middle row), conformal B (bottom row). The color bars on the right show the value of $A_t^i + B_t^i$ (left column) and H_t^i (right column) for a given tissue depth i and time step t.

logistic growth work to create the resulting checkerboard pattern which, over time, grows outward from the tumor region.
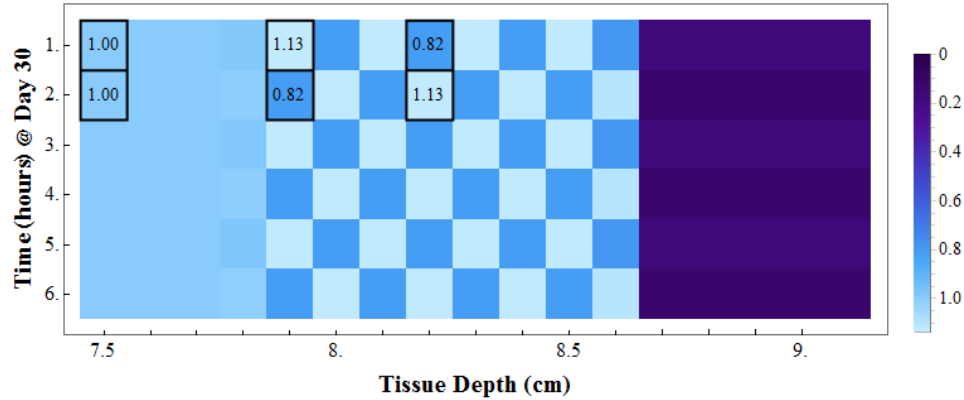

FIGURE 5. Healthy Cells (H) during the first 6 hours of Day 30 of the simulation shown in Figure 4(b). In the first and second hours, boxes have been formed around three tissue depths 7.5 cm, 7.9 cm, and 8.2 cm. The values shown in each box indicate the value of H_t^i at that time and tissue depth.

5.2. **Treatment courses with conformal proton therapy.** Since our model contains only one spatial dimension we only have the options of the proton beam originating from the left side of the spatial domain or from the right side. The simulation shown in Section 5.1 assumes that the beam is being fired from the left side of the spatial domain. To simulate the effects of conformal proton therapy where multiple modulated beams are targeted upon the tumor from different angles, we now consider simulations in which the beam is fired from both the left and right sides of the spatial domain.

Typically, when conformal proton therapy is used, the dose of each fired beam is smaller than if only a single beam is used. Recall, the data we used for the time dependent cell death rate used a 2 Gy dose and a 5 Gy dose. For the conformal proton treatment we will assume each fired beam (one from the left and one from the right) is a 2 Gy dose, giving a total dose of 4 Gy (less than was delivered in each dose in the simulation described in Section 5.1). To compare the results of the conformal treatment to the non-conformal treatment simulation of Section 5.1, we use two different treatment courses.

(A) 4 Gy total dose given 16 times over 35 days (5 weeks) as shown in Table 3(a); total of 64 Gy of proton irradiation administered
(B) 4 Gy total dose given 20 times over 49 days (7 weeks) as shown in Table 3(b); total of 80 Gy of proton irradiation administered

Note that treatment course A uses the same scheduling as was used in the Section 5.1 example, but each dose is lower (and being delivered by two 2 Gy beams). Treatment course B delivers the same amount of proton radiation but in smaller doses (and being delivered by two 2 Gy beams) and over a longer period of time.

For both of the following simulations, as with the previous simulation (Section 5.1), we assume that tissue depths with $A_t^i + B_t^i \geq 0.55$ are "visible" as a part of

the tumor, and thus contribute to the tumor diameter at time t, d_t. Additionally, the initial conditions are the same as in the previous simulation, and the results for the first 150 days (when no treatment is administered) as the same as described for the previous simulation (that is, $\boldsymbol{C_{3600}} = 2.037\boldsymbol{C_0}$ and $d_{3600} = 38$).

5.2.1. *Results of treatment course A.* The results of the simulation using treatment course A are shown in Figures 4(c) and 4(d). After the 35 day treatment period, there are 0.011 times as many cancer cells present as at Day 150 ($\boldsymbol{C_{4440}} = 0.011\ \boldsymbol{C_0}$ nearly a 99% reduction in cancer cell density), and the diameter of the visible tumor has shrunk to 0 mm ($d_{4440} = 0$). Note, that though this results is an improvement over the non-conformal treatment course described in Section 5.1, after the additional 90 day observation period, there are 1.161 times as many cancer cells present as at Day 150 ($\boldsymbol{C_{6600}} = 1.161\ \boldsymbol{C_{3600}}$, more than a 16% increase in cancer cell density when compared to right before treatment), and the diameter of the visible tumor has increased to 44 mm ($d_{6600} = 44$).

5.2.2. *Results of treatment course B.* The results of the simulation using treatment course B are shown in Figures 4(e) and 4(f). After the 49 day treatment period ($t = 4776$), there are 0.003 times as many cancer cells present as at Day 150 ($\boldsymbol{C_{4776}} = 0.003\ \boldsymbol{C_0}$ over a 99% reduction in cancer cell density), and the diameter of the visible tumor has shrunk to 0 mm ($d_{4776} = 0$). Note, that though this results is an improvement over the non-conformal treatment course described in Section 5.1 and conformal treatment course A, after the additional 90 day observation period, there are 1.154 times as many cancer cells present as at Day 150 ($\boldsymbol{C_{6936}} = 1.154\ \boldsymbol{C_{3600}}$, slightly more than a 15% increase in cancer cell density when compared to right before treatment), and the diameter of the visible tumor has increased to 44 mm ($d_{6936} = 44$).

The results for conformal treatment courses A and B are summarized in Table 4. As in the simulation described in Section 5.1, in each conformal treatment simulation the healthy cells quickly rebound into the tumor region during and shortly after treatment, but as the observation period progresses the healthy cells are removed from the tumor region as the tumor re-establishes itself.

6. **Discussion.** We have proposed a model to simulate the spatial and temporal dynamics of cancer and healthy cells before, during, and after the application of proton therapy. As an example of how the model can be applied, we have used data from in vitro clinical studies of hepatocellular carcinoma to parameterize the model, explore numerical simulations, and compare different treatment courses. Within the numerical simulations we looked at both non-conformal and conformal treatment regimes. In each of the numerical simulations the resurgence of the cancer cells and the tumor after the 90 day observation period suggest the given treatment course is not sufficient. However, there are reasons to remain hopeful.

First, note that the patient's immune response is not included in our proposed model. In the simulation of each of the three treatment courses described in Section 5, the cancer cell density directly after the treatment period was lowered to 6.2% or lower of the cell density directly before treatment was administered. For many forms of cancer, including hepatocellular carcinoma, once of the density of cancer cells is low enough, a sufficiently healthy immune system will work to remove the remaining cancer cells. This suggests a type of Allee effect (see [1], [9], and [12] for details) which causes the decay of the cancer cell population once it falls below

TABLE 4. Summary of results from all treatment courses where $t = 0$ is the initial time, t_s is the time at which the treatment course starts ($t_s = 3600$ for all treatment courses), t_e is the time at which the treatment course ends ($t_e = 4440$ for non-conformal and conformal treatment course A, and $t_e = 4776$ for conformal treatment course B), and t_o is the time at which the 90-day observation period ends ($t_o = t_e + 2160$ for all treatment courses).

		$t = 0$	t_s	t_e	t_o
Non-Conformal	Cell Density	C_0	$2.037\ C_0$	$0.062\ C_{t_s}$	$1.188\ C_{t_s}$
	Tumor Diameter	30 mm	38 mm	0 mm	44 mm
Conformal A	Cell Density	C_0	$2.037\ C_0$	$0.011\ C_{t_s}$	$1.161\ C_{t_s}$
	Tumor Diameter	30 mm	38 mm	0 mm	44 mm
Conformal B	Cell Density	C_0	$2.037\ C_0$	$0.003\ C_{t_s}$	$1.154\ C_{t_s}$
	Tumor Diameter	30 mm	38 mm	0 mm	44 mm

a certain threshold. This feature is not included in the model we proposed, but if it were, we may see the elimination of the remaining cancer cells after the proton therapy treatment course is administered.

Secondly, clinical studies show that proton therapy may be administered in conjunction with or sequentially with other forms of treatment. For example, the treatment of hepatocellular carcinomas with proton therapy may be combined with transarterial chemoembolization (TACE) [28]. The model we have proposed here simulates the effects of proton therapy used alone, not in conjunction with other therapies. We hypothesize that an extension of this model which included both proton therapy and TACE used sequentially would show improved results, possibly leading to the elimination of the cancer cells entirely.

In addition to the possible model extensions proposed above, another obvious extension would be to increases the spatial domain of this model to be three-dimensional. Increasing the spatial domain to three dimensions would allow for infinitely more possibilities in the structure of the conformal treatment courses. Other possible model extensions could be informed by the variety of cancer networks proposed by Werner, including exponential cancer networks [36, Section 6], geometric cancer networks which may provide an more accurate model of logistic growth of cancer cells at the network level [36, Section 8], linear cancer networks with stochastic dedifferentiation [36, Section 9], and cancer networks with explicitly modeled cell communication [36, Sections 11–12].

Lastly, in the simulations shown in Section 5, we considered the application of only a single treatment course. However, a patient who shows regeneration of the tumor after a given observation period would likely undergo a second treatment period. An interesting extension of this model would be to consider the optimal length of the observation period before applying a second treatment course. A clinician would need to wait long enough for the patient to recover from the first round of treatment and for there to be evidence of the tumor's regrowth, but waiting

too long could result in an even larger tumor as we saw after the 90-day observation period in the simulations in Section 5.

Both conformal treatment courses result in lower densities of cancer cells directly after the treatment period and after the 90 day observation period when compared with the non-conformal treatment course. It should be noted that since conformal treatment course A delivers a lower total amount of proton radiation (64 Gy instead of the 80 Gy) when compared to the non-conformal treatment course and conformal treatment course B, we would expect conformal treatment course A to result in fewer adverse side effects than the other two treatment courses. Additionally since both conformal treatment courses deliver better results than the non-conformal treatment course, when a conformal treatment regime is an option for a patient, our results suggest it will lead to better control of the targeted tumor. Furthermore, since both conformal treatment courses administer a lower dose on each treatment day than the non-conformal treatment course, the conformal treatment courses may be advised in patients with lower tolerances to irradiation.

As the use of proton therapy increases, the need for useful mathematical models which describe both the effectiveness of treatment and the cellular dynamics in the tissues surrounding the tumor are needed. Our model provides a tool which addresses both of these objectives and is novel in its use of both spatial and temporal dynamics in simulating the effects of proton radiation therapy. Though we have used the model here to explore the impact of proton therapy on hepatocellular carcinomas, by following the methods laid out in Section 4 one can reparameterize the model for other types of cancer. Though there are many directions in which this model could be expanded, the ability to use this model to compare different treatment courses (like the comparison of non-conformal and conformal treatment options) make this model a powerful tool.

REFERENCES

[1] W. C. Allee, Integration of problems concerning protozoan populations with those of general biology, *American Naturalist*, **75** (1941), 473–487.

[2] U. Amaldi, Particle accelerators take up the fight against cancer, *CERN Courier*, URL http://cerncourier.com/cws/article/cern/29777.

[3] L. Barbara, G. Benzi, S. Gaini, F. Fusconi, G. Zironi, S. Siringo, A. Rigamonti, C. Barabara, W. Grigioni, A. Mazziotti and L. Bolondi, Natural history of small untreated hepatocellular carcinoma in cirrhosis: A multivariate analysis of prognostic factors of tumor growth rate and patient survival, *Hepatology*, **16** (1992), 132–137.

[4] S. M. Blower, E. N. Bodine and K. Grovit-Ferbas, Predicting the potential public health impact of disease-modifying HIV vaccines in South Africa: The problem of subtypes, *Current Drug Target - Infectious Disorders*, **5** (2005), 179–192.

[5] S. Blower and H. Dowlatabadi, Sensitivity and uncertainty analysis of complex models of disease transmission: An HIV model, as an example, *International Statistical Review*, **62** (1994), 229–243.

[6] E. N. Bodine and M. V. Martinez, Optimal genetic augmentation strategies for a threatened species using a continent-island model, *Letters in Biomathematics*, **1** (2014), 23–39.

[7] T. Bortfeld, An analytical approximate of the bragg curve for therapeutic proton beams, *Medical Physics*, **24** (1997), 2024–2033.

[8] T. Bortfeld and W. Schlegel, An analytic approximation of depth-dose distributions for therapeutic proton beams, *Physics in Medicine & Biology*, **41** (1996), 1331–1339.

[9] D. Boukal and L. Berec, Single-species models of the allee effect: Extinction boundaries, sex ratios, and mate encounters, *Journal of Theoretical Biology*, **218** (2002), 375–394.

[10] W. H. Bragg and R. Kleenman, On the ionization curve of radium, *Philosophical Magazine*, **S6** (1904), 726–738.

[11] T. Chiba, K. Tokuuye, Y. Matsuzaki, S. Sugahara, Y. Chuganji, K. Kagei, J. Shoda, M. Hata, M. Abei, H. Igaki, N. Tanaka and Y. Akine, Proton beam therapy for hepatocellular carcinoma: A retrospective review of 162 patients, *Clinical Cancer Research*, **11** (2005), 3799–3805.

[12] F. Courchamp, L. Berec and J. Gascoigne, *Allee Effects in Ecology and Conservation*, Oxford Biology, Oxford University Press, 2009.

[13] F. Dionisi, L. Widesott, S. Lorentini and M. Amichetti, Is there a role for proton therapy in the treatment of hepatocellular carcinoma? A systematic review, *Radiotherapy & Oncology*, **111** (2014), 1–10.

[14] N. Fausto, Liver regeneration, *Journal of Hepatology*, **32** (2000), 19–31.

[15] A. Grajdeanu, *Modeling Diffusion in a Discrete Environment*, Technical Report GMU-CS-TR-2007-1, Department of Computer Science, George Mason University, Fairfax, VA, 2007.

[16] I. Hara, M. Murakami, K. Kagawa, K. Sugimura, S. Kamidono, Y. Hishikawa and M. Abe, Experience with conformal proton therapy for early prostate cancer, *American Journal of Clinical Oncology*, **27** (2004), 323–327.

[17] D. Jette and W. Chen, Creating a spread-out bragg peak in proton beams, *Physics in Medicine & Biology*, **56** (2011), N131–N138.

[18] R. Kjellberg, T. Hanamura, K. Davis, S. Lyons and R. Adams, Bragg-peak proton-beam therapy for arteriovenous malformations of the brain, *New England Journal of Medicine*, **309** (1983), 269–274.

[19] K. B. Lee, J.-S. Lee, J.-W. Park, T.-L. Huh and Y. Lee, Low energy proton beam induces tumor cell apoptosis through reactive oxygen species and activation of caspases, *Experimental & Molecular Medicine*, **40** (2008), 118–129.

[20] R. Levy and R. Schulte, Stereotactic radiosurgery with charged-particle beams: Technique and clinical experience, *Translational Cancer Research*, **1** (2012), 159–172.

[21] E. Lindblom, *The Impact of Hypoxia on Tumour Control Probability in the High-Dose Range Used in Stereotactic Body Radiation Therapy*, PhD thesis, Stockholm University, 2012.

[22] S. MacDonald, T. DeLaney and J. Loeffler, Proton beam radiation therapy, *Cancer Investigation*, **24** (2006), 199–208.

[23] O. Manley, A mathematical model of cancer networks with radiation therapy, *Journal of Young Investigators*, **27** (2014), 17–26.

[24] G. K. Michalopoulos and M. C. DeFrances, Liver regeneration, *Science*, **276** (1997), 60–66.

[25] N. Nagasue, H. Yukaya, Y. Ogawa, H. Kohno and T. Nakamura, Human liver regeneration after major hepatic resection; A Study of Normal Liver and Livers with Chronic Hepatitis and Cirrhosis, *Annals of Surgery*, **206** (1987), 30–39.

[26] N. Okazaki, M. Yoshino, T. Yoshida, M. Suzuki, N. Moriyama, K. Takayasu, M. Makuuchi, S. Yamazaki, H. Hasegawa, M. Noguchi and S. Hirohashi, Evalulation of the prognosis for small hepatocellular carcinoma bbase on tumor volume doubling times, *Cancer*, **63** (1989), 2207–2210.

[27] H. Paganetti and T. Bortfeld, New Technologies in Radiation Oncology, *Medical Radiology Series*, Springer-Verlag, chapter Proton Beam Radiotherapy – The State of the Art, (2006), 345–363.

[28] R. E. Schwarz, G. K. Abou-Alfa, J. F. Geschwind, S. Krishnan, R. Salem and A. P. Venook, Nonoperative therapies for combined modality treatment of hepatocellular cancer: expert consensus statement, *HPB*, **12** (2010), 313–320.

[29] R. Siegel, K. Miller and A. Jemal, Cancer statistics, 2015, *CA: A Cancer Journal for Clinicians*, **65** (2015), 5–29.

[30] J. D. Slater, C. J. J. Rossi, L. T. Yonemoto, D. A. Bush, B. R. Jabola, R. P. Levy, R. I. Grove, W. Preston and J. M. Slater, Proton therapy for prostate cancer: the initial loma linda university experience, *International Journal of Radiation Oncololy Biology Physics*, **59** (2004), 348–352.

[31] A. Terahara, A. Niemierko, M. Goitein, D. Finkelstein, E. Hug, N. Liebsch, D. OFarrell, S. Lyons and J. Munzenrider, Analysis of the relationship betwen tumor dose inhomogeneity and local control in patients with skull base chordoma, *International Journal of Radiation Oncololy Biology Physics*, **45** (1999), 351–358.

[32] M. Tubiana, Tumor cell proliferation kinetics and tumor growth rate, *Acta Oncologica*, **28** (1989), 113–121.

[33] W. Ulmer and B. Schaffner, Foundation of an analytical proton beamlet model for inclusion in a general proton dose calculation system, *Radiation Physics and Chemistry*, **80** (2011), 378–389.

[34] D. Weber, A. Trofimov, T. DeLaney and T. Bortfeld, A treatment plan comparison of intensity modulated photon and proton therapy for paraspinal sarcomas, *International Journal of Radiation Oncoloy Biology Physics*, **58** (2004), 1596–1606.

[35] U. Weber and G. Kraft, Comparison of carbon ions vs protons, *The Cancer Journal*, **15** (2009), 325–332.

[36] E. Werner, A general theoretical and computational framework for understanding cancer, arXiv:1110.5865.

[37] R. Wilson, Radiological use of fast protons, *Radiology*, **47** (1946), 487–491.

[38] J. F. Ziegler, The stopping of energetic light ions in elemental matter, *Journal of Applied Physics*, **85** (1999), 1249–1272.

E-mail address: bodinee@rhodes.edu

E-mail address: klmonia0001@training.navy.mil